Magnetic structure of oxygen-deficient perovskite nickelates with ordered vacancies

Yongjin Shin and James M. Rondinelli* Department of Materials Science and Engineering, Northwestern University, Evanston IL, 60208, USA

The oxygen vacancy concentration in LaNiO_{3- δ} nickelate perovskites affects magnetic interactions and long-range magnetic order through changes in local electronic configurations, crystal field splitting energies, and polyhedral arrangements. Here we use density functional theory calculation to examine the magnetic structure of LaNiO_{2.5} and LaNiO_{2.75} with structural ordered oxygen-vacancies (OOV). These OOV phases exhibit columnar arrangements of NiO₄ square planar units, which adopt low-spin Ni²⁺ (d^8) configurations with nominally zero magnetic moment (S=0), interconnected by NiO₆ octahedral units. The magnetic structure of the OOV phases are governed by the flexible charge state of the NiO₆ octahedral units, whose density and connectivity depends on the oxygen vacancy concentration. LaNiO_{2.5} is stable in an insulating A-type antiferromagnetic (AFM) phase derived from octahedral units comprising Ni²⁺ in AFM chains. LaNiO_{2.75} is a narrow-gap insulator with zigzag-type AFM order originating from weakly localized electrons in columnar breathing distortions to the NiO₆ units. Our results suggest that nanoscale OOV phases within single phase LaNiO_{3- δ} crystals can account for its reported complex magnetic ground state structure.

Rare-earth nickelate perovskites, $R \text{NiO}_3$, are a family of compounds that exhibits temperature-dependent metal-insulator transition (MIT) [1–3]. The antiferromagnetic (AFM) ground state at lower temperature is realized by nominal charge disproportionation of Ni^{3+} to Ni^{2+} and Ni^{4+} , associated with rocksalt-type breathing distortions of the corner-connected octahedra [4, 5]. The breathing distortion stability depends on the degree of in-phase rotation and tilting distortion, which affects MIT transition temperature as described in phase diagrams based on R radii or crystallographic tolerance factors [6]. LaNiO₃ with its large tolerance factor exhibits $R\bar{3}c$ symmetry unlike the monoclinic nickelates, which prohibits the breathing distortion [7, 8], and accounts for his broad temperature dependent paramagnetic metallic behavior.

Formation of oxygen vacancies in LaNiO₃ and its impact on the electronic/magnetic structure has drawn renewed particular interest. First, understanding magnetism of the oxygen-deficient phases is useful for intrepretating the magnetic state of LaNiO₃ crystals synthesized with various methods [9–12]. Indeed, along the vacancy-driven transitions in LaNiO_{3- δ} for δ from 0 to 0.5, a significant change of properties occurs in both electronic (metal-semiconductor-insulator) and magnetic (paramagnetic-ferromagnetic-antiferromagnetic) properties [13, 14]. In addition, the end member of this transition, the infinite-layer RNiO₂ family, hosts superconductivity [15, 16].

The formation of ordered-oxygen vacancies (OOVs) is observed in oxygen-deficient phases, and it transforms ${\rm NiO_6}$ octahedra to ${\rm NiO_4}$ square planar units as shown in Fig. 1 [14]. The change in coordination number (reduced bandwidth) and electron filling explains the insulating AFM properties of LaNiO_{2.5} found both in experiment and first-principles calculations [10, 17–19]. On the other hand, less understanding exists for intermediate oxygen deficiencies between LaNiO₃ and LaNiO_{2.5}, which have been interpreted as transient states with statistical distributions of oxygen vacancies [14, 20], mainly because of limited knowledge of therir atomic structures.

Here we perform density functional theory (DFT) calculations to identify and assess stable atomic structures and the corresponding electronic/magnetic properties of $LaNiO_{2.5}$ and $LaNiO_{2.75}$ with OOVs (Fig. 1). We find that out-of-phase rotations of octahedra (like those in the $R\bar{3}c$ perovskite phase) are the most stable distortion occurring in the OOV phases. The Pnma-like distortion (with inphase rotations) energetically competes with them. Furthermore, we show the physical properties are determined by the Ni valence in the NiO₆ octahedral units, as Ni in the square planar unit remains diamagnetic throughout with a low-spin $Ni^{2+}(d^8, S=0)$ configuration. In LaNiO_{2.5}, the octahedral units adopt high-spin Ni²⁺ (d^8 , S=1) configurations and form antiferromagnetic chains along the c direction, stabilizing an A-type AFM insulator. In contrast, LaNiO_{2.75} exhibits columnar breathing distortions of octahedra, owing to the internal strain induced by the linking NiO₄ units. This structure connectivity stabilizes charge ordering and a zigzag AFM order with a narrow band gap. Finally, we argue that the magnetic properties observed in LaNiO_{3- δ} with $0 \le \delta \le 0.5$ can be understood as arising from OOVs rather than random oxygen-vacancy distributions.

We used the Vienna Ab-initio Simulations Package (VASP) [21, 22] to perform our DFT calculations with the Perdew-Burke-Ernzerhof functional (PBE)[23]. Projectoraugmented wave (PAW) potentials [24] were used to describe the electron core-valence interactions with the following configurations: La $(4f^05s^25p^65d^16s^2)$, Ni $(3d^94s^1)$, and O $(2s^22p^4)$. A 550 eV planewave cutoff was used to obtain the ground structure for each composition. Brillouin zone integrations employed the tetrahedron method [25], based on a Monkhorst-Pack k-point mesh obtained using the K-point grid server with 34 Å of minimum distance between lattice points [26, 27]. The cell volume was relaxed and atomic positions were evolved until the forces on each atom were less than 1 meV Å^{-1} . We adopted the plus Hubbard U correction [28] of 1.5 eV for the correlated Ni 3d orbitals [5, 29, 30]. The effect of U on the

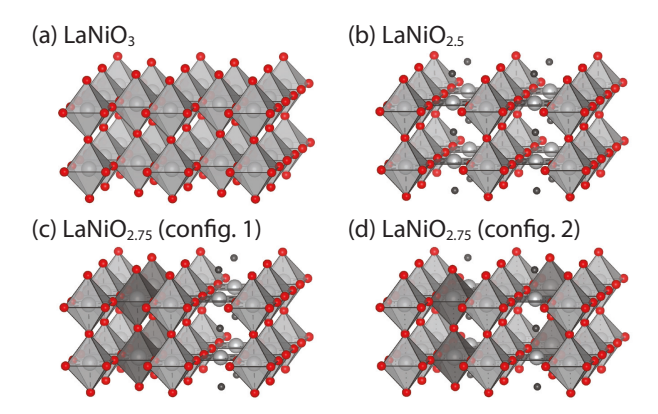


FIG. 1. Structures of vacancy ordered LaNiO $_{3-\delta}$ with varying oxygen vacancy content. (a) LaNiO $_3$, (b) LaNiO $_{2.5}$, (c) LaNiO $_{2.75}$ (config. 1), and (d) LaNiO $_{2.75}$ (config. 2). La atoms are omitted and vacancies are drawn as gray spheres for a better description. Octahedral units with smaller volumes are highlighted with darker shading.

formation energy and magnetic stabilities is discussed in the Supplementary Information (SI) [31].

Data from the literature describe the atomic structures of LaNiO_{2.5} and LaNiO_{2.75} as comprising OOVs in the [110] pseudocubic (pc) direction, forming NiO₆ and NiO₄ chains along c-axis as illustrated in Fig. 1 [32]. The inherently lower symmetry of the OOV phases compared to stoichiometric perovskites leads to higher complexity in potential distortion patterns. To efficiently survey the stable distortion patterns, we identified the rotation/tilting modes responsible for the two energy-competing space groups in RNiO₃: $a^-a^-a^-$ ($R\bar{3}c$) and $a^+a^-c^-$ (Pnma) [33]. The modes include (i) out-of-phase rotation ($a^-b^0b^0$), (ii) in-phase rotation ($a^+b^0b^0$), and (iii) tilting of apical oxygens ($a^0b^-b^-$). These modes were identified from ideal (non-distorted) structures using PHONOPY [34] and ISODISTORT [35, 36].

When OOVs are introduced into $\text{LaNiO}_{3-\delta}$, the $\text{LaNiO}_{2.5}$ structure exhibits a checkerboard ordering of NiO_4 and NiO_6 columns on the $(001)_{pc}$ plane. Much less is known about the atomic structure of $\text{LaNiO}_{2.75}$ [37–39], which is conjectured to be an intermediate stoichiometric phase between $\text{LaNiO}_{2.5}$ and LaNiO_3 . Based on the preference of vacancies to form square planar units [40] and diffraction peaks near the boundary between $\text{LaNiO}_{2.5}$ and LaNiO_3 [10], we deduced that $\text{LaNiO}_{2.75}$ possesses fewer NiO_4 columns than $\text{LaNiO}_{2.5}$. The NiO_4 columns are replaced with columns of NiO_6 octahedra. This change in coordination led us to construct two distinct configurations (config. 1 and 2) for $\text{LaNiO}_{2.75}$. The configurations are distinguished by the cis or trans alignment of NiO_4 columns as illustrated in Fig. 1(c, d).

Adding OOVs to perovskite lowers the cubic symmetry to either tetragonal or orthorhombic: P4/mmm (LaNiO_{2.5}), Pmmm (LaNiO_{2.75}; config. 1), and P4/mmm (LaNiO_{2.75}; config. 2). This anisotropic nature of OOV phases makes Glazer notation [41], which is used to describe octahedral rotations in perovskites relative to a

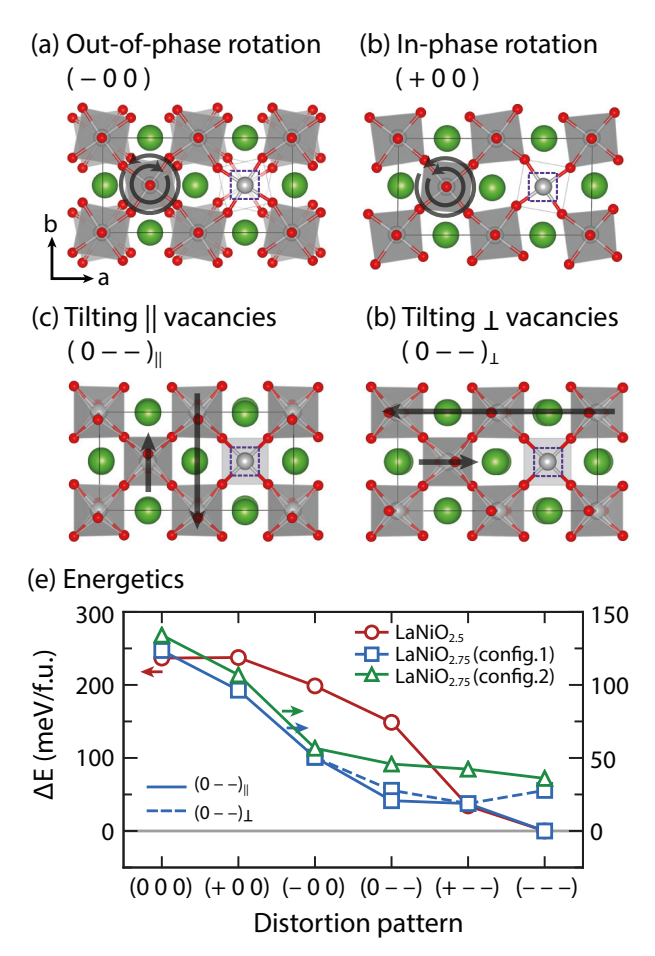


FIG. 2. Major distortion modes in (a-d) LaNiO_{2.75} (config. 1): out-of-phase rotation, in-phase rotation, tilting of apical oxygen atoms parallel/perpendicular to the ordered vacancies. For LaNiO_{2.5} and LaNiO_{2.75} (config. 2), the two tilting modes are symmetrically identical. (e) Relative energies with different distortion patterns in LaNiO_{3- δ} phases with OOVs based on nonspin-polarized calculations.

set of Cartesian axes, not directly applicable. Here, we adopted a modified notation as follows: non-distorted (0), in-phase rotation (+), and out-of-phase rotations (–) as illustrated in Fig. 2. The orthorhombic parent structure of LaNiO_{2.75} (config. 1) permits two different types of tilting modes about directions relative to the OOVs forming the NiO₄ units: $(0 - -)_{||}$ and $(0 - -)_{\perp}$ corresponding to the direction of apical oxygen tilting parallel (||) or perpendicular (\perp) to the NiO₄ layer, respectively, as shown in Fig. 2(c,d). The detailed group theoretical analysis of the tilt-symmetry breaking is described in the SI [31].

Fig. 2 shows the general energetics for different distortions without magnetic interactions. For all phases, the out-of-phase (0 - -) tilting mode is more energetically favorable than either of the single in-phase or out-of-phase rotation modes. The lowest energy configurations are obtained by combination of either one of these single rotation modes, (+00) or (-00), with the tilting mode. Between the (+--) and (---) patterns, we found the

(---) type pattern is lower in energy: $34.3\,\mathrm{meV/f.u.}$ for LaNiO_{2.5}, $18.7\,\mathrm{meV/f.u.}$ for LaNiO_{2.75} (config. 1) and $6.34\,\mathrm{meV/f.u.}$ for LaNiO_{2.75} (config. 2). For LaNiO_{2.75} config. 1, the $(0\,--)_{||}$ tilt is energetically prefered to the $(0\,--)_{\perp}$ tilt, and it is more stable than config. 2 by $36\,\mathrm{meV/f.u.}$ This energy difference arises from the $(0\,--)_{\perp}$ tilting, where oxygen atoms briding square planar units are symmetrically locked along the vacancy plane direction (||). This locking makes it difficult to relax the strain induced by the oxygen vacancies, resulting in relatively higher energy.

Next, we to study the effect of spin-polarization on the energetics in Fig. 2. Although the relative energetics change, the overall trend is the same as that obtained from the nonspin-polarized calculations. Note that the stable reference spin configurations are A-AFM for $LaNiO_{2.5}$ and FM for LaNiO_{2.75}; a detailed discussion of these magnetic states is given further below. First, the energy difference between the (+--) and (---) patterns is significantly reduced: $0.24 \,\mathrm{meV/f.u.}$ for $\mathrm{LaNiO}_{2.5}$, $9.8 \,\mathrm{meV/f.u.}$ for $LaNiO_{2.75}$ (config. 1) and $2.8 \, meV/f.u.$ for $LaNiO_{2.75}$ (config. 2). In addition, the energy difference between config. 1 and 2 is reduced further to less than 2 meV/f.u., indicating the strength of the magnetic interactions is comparable to the difference from elastic strain effects in the (+--)and (---) octahedral patterns (SI) [31]. There is an approximate 10% difference between the equatorial and apical Ni-O bond distances, regardless of the distortion patterns, in the octahedral units in OOV phases which presents like a compressed Jahn-Teller distortion, i.e., the equatorial bond length is longer than apical bond length. This distortion mainly originates from the significantly shorter Ni–O bond lengths in the NiO₄ units [32]. The bond length differences shifts the bridging oxygen between the NiO₆ and NiO₄ closer to to the NiO₄ unit, which elongates the octahedral unit in the ab-plane. For LaNiO_{2.75}, a similar distortion is found within the larger octahedra whereas the smaller octahedra exhibit almost isotropic bond lengths (darker octahedra in Fig. 1). This Jahn–Teller-like distortion is distinguished from the conventional first-order Jahn-Teller distortion found in d^4 LaMnO₃, as the high-spin d^8 configuration within an octahedral crystal frield lacks any orbital degenerate as discussed further below.

Our phonon calculations with spin-polarization confirmed the dynamic stabilities of the (---) and (+--) patterns for LaNiO_{2.5} and LaNiO_{2.75} (config. 1) [31] with symmetries specified in Table I. The ground state C2/c space group of LaNiO_{2.5} agrees with the experimentally reported atomic structure [37–39]. In addition, we identified that the metastable structure with the (+--) tilt pattern and $P2_1/m$ space group is close in energy to the ground state phase. Our phonon calculations for LaNiO_{2.75} config. 1 further confirm that the $(---)_{\perp}$ tilt is dynamically unstable; any atomic perturbation drives the structure to relax into the $(---)_{\parallel}$ tilt, which is then adopted and becomes the dynamically stable ground states (P2/c). Note that adding the (+0.0) mode to

TABLE I. Summary of electronic and structural information of OOV LaNiO $_{3-\delta}$ phases. Electronic configuration of nickel atoms are provided based on polyhedral units, and space group of stable derivative OOV nickelates are listed. The structures of LaNiO $_{2.75}$ with Config. 2 are dynamically unstable.

| Features | $LaNiO_{2.5}$ | $LaNiO_{2.75}$ | |
|-----------------------|---|---|--|
| d-filling | Oct. / Square d^8 / d^8 $S = 1$ / $S = 0$ | Oct. (L) / Oct. (S) / Sq d^{8} / d^{6} / $S = 1$ / $S = 0$ / S | $ \begin{array}{l} \text{uare} \\ d^8 \\ = 0 \end{array} $ |
| | | $\text{LaNiO}_{2.75}$ | |
| Tilt | $LaNiO_{2.5}$ | Config. 1 Config. 2 | ; |

 $P2_1/m$

P2/c

 $P2_1/m$

C2/c

 $P2_1/m$

C2/c

either $(0--)_{\perp}$ or $(0--)_{||}$ gives the same symmetry reduction, i.e., a $P2_1/m$ space group. This is not the case when adding the (-00) to those two-tilt systems. Although both $(---)_{\perp}$ and $(---)_{\parallel}$ patterns exhibit the P2/c space group, their tilting directions differ with respect to the vacancy plane. This difference leads to the $(---)_{||}$ pattern as the lowest energy and dynamically stable distortion (Table I). On the other hand, the inphase rotation mode in config. 1 removes the symmetric difference between the two tilting modes, where single (+--)-type pattern is obtained with the dynamically stable $P2_1/m$ space group. For config. 2 of LaNiO_{2.75}, both (---) and (+--) distortions are dynamically unstable solutions. Modulating these two structures along the unstable distortions yields triclinic $P\bar{1}$ symmetry resembling the (---) distortion, but with higher anisotropy of Ni-O bond lengths in the *ab*-plane.

To identify the ground state magnetic structure of LaNiO_{2.5}, we examined the energetic stabilities of different magnetic orders with the (---) distortion that gives C2/c symmetry. We found A-type AFM is the most stable and leads to an insulating gap of $\sim 0.75 \, \text{eV}$ (Fig. 3). The calculated magnetic moments are $1.5 \mu_B$ and $0.15 \mu_B$ for Ni²⁺ in the NiO₆ and NiO₄ units, respectively, which indicates each unit stabilizes high-spin $(d^8, S = 1)$ and low-spin $(d^8, S = 0)$ configurations. Our assignment of a low-spin configuration for the NiO₄ unit is also supported by its short Ni–O bond lengths of 1.88 Å that give a strong crystal field splitting effect [42]. The stability of A-type AFM order is consistent with the Goodenough-Kanamori-Anderson (GKA) superxchange rules for these orbital fillings [43, 44]. As both e_q states of the octahedral unit are half-filled, the linear octahedral chains along c are AFM coupled to one another. The low-spin configuration on NiO₄ units are diamagnetic so their magnetic coupling is negligible. This leads to the small energy difference of 3.28 meV/f.u. between the A- and A⁻-type orders, where A⁻-AFM possesses both spin up/down octahedral units on same ab-plane as depicted in Fig. 3(a).

Our discussion of the magnetic structure of LaNiO $_{2.75}$ focuses on the monoclinic phase with config. 1 and the

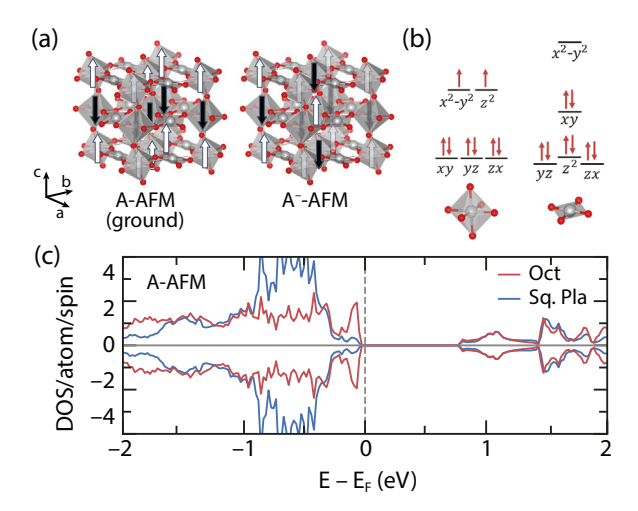


FIG. 3. (a) Stable magnetic orders in $LaNiO_{2.5}$. La atoms are omitted. (b) Electronic filling of the octahedral and square planar units. (c) Density of states (DOS) per Ni atom.

(---) tilt distortion (P2/c). The ground state is a narrow gap insulator $(E_q \sim 0.1 \, \text{eV})$ with zigzag AFM order $(E_a$ -AFM), as illustrated in Fig. 4. Although the orbital structure of NiO₄ unit is similar to that in LaNiO_{2.5}, the Ni of the octahedral units in LaNiO_{2.75} make the Ni states near E_F significantly more dispersive compared to insulating LaNiO_{2.5}. Interestingly, the band gap is sensitive to the magnetic order imposed. The zigzag spin order perpendicular to vacancy plane (E_a) gives an insulating state whereas a zigzag spin order parallel to the vacancy plane (E_b) gives a metallic solution that is $\sim 6.6 \,\mathrm{meV/f.u.}$ higher in energy than insulating solution. The zigzag E-type order includes both FM and AFM coupling between large and small octahedral units, similar to magnetic solutions in the $RNiO_3$ family with rock-salt breathing distortions that support an insulating state [5]. In this regard, metallicity in LaNiO_{2.75} may arise from either vacancy or magnetic order is disrupted. We also tested other zigzag magnetic orders (S- and T-AFM from Ref. 5) and found energetically competing solutions; a quantitative comparison of magnetic stabilities and their U-value dependence is made in SI [31].

We found the E-type AFM is associated with columnar breathing distortion in LaNiO_{2.75}, which realizes charge ordering between large (light) and small (dark) octahedral units in Fig. 4. This behavior is not possible in LaNiO_{2.5} owing to Ni²⁺ occupying both NiO₆ and NiO₄ units (Table I). The magnetic moments of the large and small octahedra are $1.2\,\mu_B$ and $0.7\,\mu_B$, respectively, implying considerable charge disproportionation. Although the effective charge states are close to 2.5+ and 3+, they can be nominally assigned as Ni²⁺ and Ni⁴⁺ considering the significant degree of Ni–O hybridization, which agrees with ligand-associated charge ordering [45]. We attribute the origin of the columnar breathing distortion to the internal strain induced by NiO₄ unit: the octahedral units on similar sites with NiO₄ units are subjected to compres-

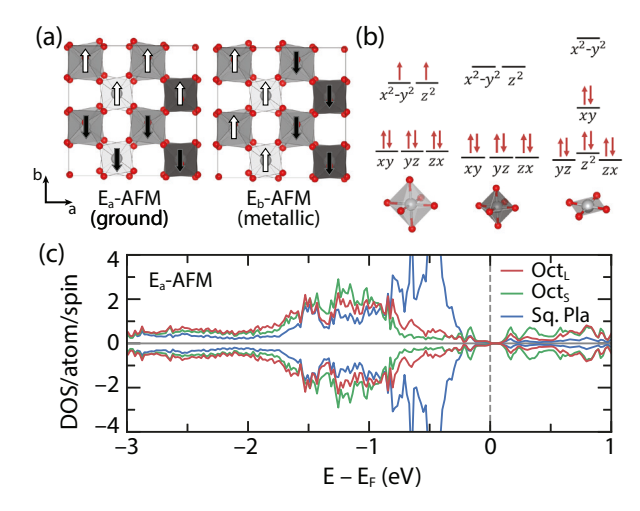


FIG. 4. (a) Stable magnetic orders in LaNiO_{2.75}. La atoms are omitted. (b) Electronic filling of the octahedral and square planar units. (c) Density of states (DOS) per Ni atom.

sive stresses to stabilize a similar level of bond valence with the NiO₄ units. The local Ni magnetic moment in the NiO₄ unit is $0.03\,\mu_B$, which indicates the strong preference toward low-spin Ni²⁺ (d^8 , S=0). Thus, the breathing distortion is driven from 'stiff' NiO₄ units in LaNiO_{2.75}. The charge ordering among Ni sites in the LaNiO_{2.75} octahedra also occurs regardless of the metallic or magnetic order adopted.

The columnar arrangement of breathing distortion in LaNiO_{2.75} is uniquely distinguished from that found in other RNiO₃ compounds. While rock-salt ordering of large/small octahedral units in RNiO₃ makes 6 connections for each octahedron to octahedral units of the other size, LaNiO_{2.75} leaves connections between equivalent type of octahedra along the c-axis with the number of smaller octahedra half the number of the larger units. With this unique arrangement, we also expect $LaNiO_{2.75}$ to possibly host novel phenomena with its unique electronic structure. First, a low-dimensional electron gas may be found above its MIT temperature where the narrow band gap is closed. Our DFT calculation predicts the metallic phase with AFM order is more stable than the FM spin orfer owing to the columnar breathing distortion. These AFM metals exhibit a low-dimensional electron gas, as shown in Fermi surface included in the SI [31], because electronic conduction is limited by the magnetic order and the NiO₄ planes. Secondly, the zigzag AFM order lifts inversion symmetry in the P2/c space group, enabling multiferroic behavior in LaNiO_{2.75}. The polar magnetic space groups are $P_b 2_1$ and Pc' for E_a - and E_b -AFM order, respectively, at the collinear-spin level, whereas noncollinear spins are required for multiferroicity in LaNiO₃ [46].

Coexistence of LaNiO_{2.75} with perovskite LaNiO₃ may in part explain the unique behavior in LaNiO_{3- δ}. For instance, a breathing distortion in LaNiO_{3- δ} was reported based on pair distribution (PDF) measurements [47]. The breathing distortion was attributed to the $P2_1/n$ space group like other low-temperature RNiO₃ structures. mainly because of the monoclinic feature appearing in the PDF data. The existence of LaNiO_{2.75} was rejected despite the presence of oxygen vacancies because LaNiO_{2.75} was previously reported in a triclinic rather than monoclinic structure [20]. Our work reveals that a monoclinic LaNiO_{2.75} structure with columnar breathing distortion is energetically and dynamically stable, and its structure may better describe the local displacements observed experimentally in LaNiO_{3- δ}. To discern the origin of the breathing distortions, we suggest analyses on the arrangement of the smaller octahedral units or the relative proportion of octahedra with different sizes. Because of the 2:1 ratio of large to small octahedra, we expect different peak-height ratios in X-ray absorption spectra of $LaNiO_{2.75}$ compared to spectra of $RNiO_3$; furthermore, lower-dimensional features may appear in angle-resolved photoemission spectrum on single crystals of LaNiO_{2.75} that could confirm its electronic description (see band structures in SI [31]).

Given our understanding now of the electronic structure of LaNiO_{2.75}, we now interpret the magnetic/electronic transitions found in LaNiO_{3- δ}. Along the magnetic (PM-FM-AFM) and electronic (metal-semiconductor-insulator) transitions in the LaNiO_{3- δ} ($0 \le \delta \le 0.5$) series [13, 14], the end-member phase $\text{LaNiO}_{2.5}$ best explains the AFM insulating state. On the other hand, the intemediatemember LaNiO_{2,75} does not directly agree with the observed FM/semiconducting behavior. Noting that the ground state of LaNiO_{2.75} is an AFM insulator with a narrow-gap, we attribute the FM/semiconducting behavior to either a distruption of the vacancy order and/or disruption of the magnetic structure. When the structural vacancy order is imperfect, the formation of NiO₄ units reduces the number of states near E_F and inhibits electronic hopping, and clustered octahedral units would adopt either Ni²⁺ or Ni³⁺, which spontaneously stabilizes FM spin coupling. This view is supported by a LaNiO_{2.75} report finding that the sign of $\partial \sigma / \partial T$ changes from semiconductor to correlated metal when thermally annealed [14], where considerable re-distribution of oxygen vacancies is expected. However, we expect the formation of NiO₄ units are still prefered even when the vacancy order is disrupted as we find that Config. 1 of LaNiO_{2.75} is relatively more stable than other arrangements of oxygen vacancies,

including the possibility of square pyramidal coordination (NiO₅ units) and randomly distributed vacancies, as discussed in the SI [31]. On the other hand, finite temperature might stabilize FM order over zigzag-type magnetic orders. The FM order is 16 meV/f.u. higher than the ground state [31], which may be thermally surmountable and could represent the FM feature observed in some LaNiO_{3- δ} crystals [10]. We additionally note that interfacial effects from LaNiO_{2.75}/LaNiO_{2.5} or LaNiO_{2.75}/LaNiO₃ junctions may also play a role, especially because single crystal $\text{LaNiO}_{2.75}$ has not been investigated without phase fractions of LaNiO_{2.5} and LaNiO₃. Thus, we anticipate further experimental work dedicated to synthesis and property measurments of single phase LaNiO_{2.75} would help create a more complete view of topotactic transitions in $\text{LaNiO}_{3-\delta}$ and the range of phenomena accessible in complex nickelates.

We identified the detailed electronic/magnetic structure of oxygen-deficient LaNiO_{3- δ} with ordered oxygen vacancies (OOV). OOV in nickelate perovskites forms NiO_4 square planar units along $(110)_{pc}$ plane, which stabilizes low-spin Ni²⁺ (d^8 , S=0) configuration. While this units become magnetically inactive, they tunes the charge states of octahedral units which determine the magnetism of the OOV phases. For insulating LaNiO_{2.5}, the octahedral units exhibit high-spin Ni²⁺ (d^8 , S=1) and their structure along the c direction favors AFM coupling and stabilizes A-AFM order. The semiconducting LaNiO_{2.75} phase with a more complicated atomic structure comprising square planar units and dilated/contracted octahedral units. The columnar breathing distortion of octahedral units host charge disproportionation of Ni atoms to nominally Ni²⁺ and Ni⁴⁺ with zigzag-type AFM orders. The identified OOV phases explain electronic/magnetic properties with varying oxygen contents, and also contributes to unique magnetic behavior of LaNiO_{3- δ} crystals.

Y.S. and J.M.R. acknowledge support from the National Science Foundation (NSF) under award number DMR-2011208. Calculations were performed using the QUEST HPC Facility at Northwestern, the Extreme Science and Engineering Discovery Environment (XSEDE), which is supported by the National Science Foundation under Grant No. ACI-1548562, and the Center for Nanoscale Materials (Carbon) Cluster, an Office of Science user facility supported by the U.S. Department of Energy, Office of Science, Office of Basic Energy Sciences, under Contract No. DE-AC02-06CH11357.

^{*} irondinelli@northwestern.edu

J. B. Torrance, P. Lacorre, A. I. Nazzal, E. J. Ansaldo, and C. Niedermayer, Systematic study of insulator-metal transitions in perovskites RNiO₃ (R=Pr, Nd, Sm, Eu) due to closing of charge-transfer gap, Phys. Rev. B 45, 8209 (1992).

^[2] J. A. Alonso, J. L. García-Muñoz, M. T. Fernández-Díaz, M. A. G. Aranda, M. J. Martínez-Lope, and M. T. Ca-

sais, Charge disproportionation in $RNiO_3$ perovskites: Simultaneous metal-insulator and structural transition in $YNiO_3$, Phys. Rev. Lett. **82**, 3871 (1999).

^[3] M. L. Medarde, Structural, magnetic and electronic properties of $RNiO_3$ perovskites (R = rare earth), Journal of Physics: Condensed Matter 9, 1679 (1997).

^[4] A. Mercy, J. Bieder, J. Íñiguez, and P. Ghosez, Structurally triggered metal-insulator transition in rare-earth

- nickelates, Nature Communications 8, 1677 (2017).
- [5] J. Varignon, M. N. Grisolia, J. Íñiguez, A. Barthélémy, and M. Bibes, Complete phase diagram of rare-earth nickelates from first-principles, npj Quantum Materials 2, 21 (2017).
- [6] N. Wagner, D. Puggioni, and J. M. Rondinelli, Learning from correlations based on local structure: Rare-earth nickelates revisited, Journal of Chemical Information and Modeling 58, 2491 (2018).
- [7] S. Lee, R. Chen, and L. Balents, Landau theory of charge and spin ordering in the nickelates, Phys. Rev. Lett. 106, 016405 (2011).
- [8] S. Lee, R. Chen, and L. Balents, Metal-insulator transition in a two-band model for the perovskite nickelates, Phys. Rev. B 84, 165119 (2011).
- [9] J. Zhang, H. Zheng, Y. Ren, and J. F. Mitchell, Highpressure floating-zone growth of perovskite nickelate LaNiO₃ single crystals, Crystal Growth & Design 17, 2730 (2017).
- [10] B.-X. Wang, S. Rosenkranz, X. Rui, J. Zhang, F. Ye, H. Zheng, R. F. Klie, J. F. Mitchell, and D. Phelan, Antiferromagnetic defect structure in LaNiO_{3-δ} single crystals, Phys. Rev. Materials 2, 064404 (2018).
- [11] K. Dey, W. Hergett, P. Telang, M. M. Abdel-Hafiez, and R. Klingeler, Magnetic properties of high-pressure optical floating-zone grown LaNiO₃ single crystals, Journal of Crystal Growth 524, 125157 (2019).
- [12] H. Guo, Z. W. Li, L. Zhao, Z. Hu, C. F. Chang, C.-Y. Kuo, W. Schmidt, A. Piovano, T. W. Pi, O. Sobolev, D. I. Khomskii, L. H. Tjeng, and A. C. Komarek, Antiferromagnetic correlations in the metallic strongly correlated transition metal oxide LaNiO₃, Nature Communications 9, 43 (2018).
- [13] T. Moriga, O. Usaka, I. Nakabayashi, T. Kinouchi, S. Kikkawa, and F. Kanamaru, Characterization of oxygen-deficient phases appearing in reduction of the perovskite-type LaNiO₃ to La₂Ni₂O₅, Solid State Ionics 79, 252 (1995).
- [14] R. D. Sánchez, M. T. Causa, A. Caneiro, A. Butera, M. Vallet-Regí, M. J. Sayagués, J. González-Calbet, F. García-Sanz, and J. Rivas, Metal-insulator transition in oxygen-deficient LaNiO_{3-x} perovskites, Phys. Rev. B 54, 16574 (1996).
- [15] A. S. Botana and M. R. Norman, Similarities and Differences between LaNiO₂ and CaCuO₂ and Implications for Superconductivity, Phys. Rev. X 10, 011024 (2020).
- [16] D. Li, K. Lee, B. Y. Wang, M. Osada, S. Crossley, H. R. Lee, Y. Cui, Y. Hikita, and H. Y. Hwang, Superconductivity in an infinite-layer nickelate, Nature 572, 624 (2019).
- [17] M. Kotiuga, Z. Zhang, J. Li, F. Rodolakis, H. Zhou, R. Sutarto, F. He, Q. Wang, Y. Sun, Y. Wang, N. A. Aghamiri, S. B. Hancock, L. P. Rokhinson, D. P. Landau, Y. Abate, J. W. Freeland, R. Comin, S. Ramanathan, and K. M. Rabe, Carrier localization in perovskite nickelates from oxygen vacancies, Proceedings of the National Academy of Sciences 116, 21992 (2019).
- [18] D. Misra and T. K. Kundu, Oxygen vacancy induced metal-insulator transition in LaNiO₃, The European Physical Journal B 89, 10.1140/epjb/e2015-60714-0 (2016).
- [19] X. Liao, V. Singh, and H. Park, Oxygen vacancy induced site-selective mott transition in lanio₃, Phys. Rev. B 103, 085110 (2021).
- [20] J. M. González-Calbet, M. J. Sayagués, and M. Vallet-

- Regí, An electron diffraction study of new phases in the LaNiO_{3-x} system, Solid State Ionics **32-33**, 721 (1989).
- [21] G. Kresse and J. Furthmüller, Efficient iterative schemes for ab initio total-energy calculations using a plane-wave basis set, Phys. Rev. B 54, 11169 (1996).
- [22] G. Kresse and D. Joubert, From ultrasoft pseudopotentials to the projector augmented-wave method, Phys. Rev. B 59, 1758 (1999).
- [23] J. P. Perdew, K. Burke, and M. Ernzerhof, Generalized gradient approximation made simple, Phys. Rev. Lett. 77, 3865 (1996).
- [24] P. E. Blöchl, Projector augmented-wave method, Phys. Rev. B 50, 17953 (1994).
- [25] P. E. Blöchl, O. Jepsen, and O. K. Andersen, Improved tetrahedron method for Brillouin-zone integrations, Phys. Rev. B 49, 16223 (1994).
- [26] H. J. Monkhorst and J. D. Pack, Special points for Brillouin-zone integrations, Phys. Rev. B 13, 5188 (1976).
- [27] P. Wisesa, K. A. McGill, and T. Mueller, Efficient generation of generalized Monkhorst-Pack grids through the use of informatics, Phys. Rev. B 93, 155109 (2016).
- [28] S. L. Dudarev, G. A. Botton, S. Y. Savrasov, C. J. Humphreys, and A. P. Sutton, Electron-energy-loss spectra and the structural stability of nickel oxide: An LSDA+U study, Phys. Rev. B 57, 1505 (1998).
- [29] A. Hampel and C. Ederer, Interplay between breathing mode distortion and magnetic order in rare-earth nickelates rnio₃ within DFT + U, Phys. Rev. B 96, 165130 (2017).
- [30] A. Hampel, P. Liu, C. Franchini, and C. Ederer, Energetics of the coupled electronic-structural transition in the rare-earth nickelates, npj Quantum Materials 4, 5 (2019).
- [31] See Supplemental Material at [URL will be inserted by publisher] for additional computational details including crystal structure information, phonon band structure, density of states of other derivative structures.
- [32] S. Estradé, F. Sánchez, G. Herranz, D. Pesquera, J. M. Rebled, N. Dix, M. J. Casanove, L. López-Conesa, C. Magén, J. Fontcuberta, and F. Peiró, Evidence of a minority monoclinic LaNiO_{2.5} phase in lanthanum nickelate thin films, Physical Chemistry Chemical Physics 19, 9137 (2017).
- [33] A. Subedi, Breathing distortions in the metallic, antiferromagnetic phase of LaNiO₃, SciPost Phys. 5, 20 (2018).
- [34] A. Togo, F. Oba, and I. Tanaka, First-principles calculations of the ferroelastic transition between rutile-type and CaCl₂-type SiO₂ at high pressures, Phys. Rev. B 78, 134106 (2008).
- [35] H. T. Stokes, D. M. Hatch, and B. J. Campbell, ISODIS-TORT, ISOTROPY Software Suite, iso.byu.edu.
- [36] B. J. Campbell, H. T. Stokes, D. E. Tanner, and D. M. Hatch, *ISODISPLACE*: a web-based tool for exploring structural distortions, Journal of Applied Crystallography 39, 607 (2006).
- [37] J. A. Alonso, M. J. MartinezLope, J. L. GarciaMunoz, and M. T. FernandezDiaz, A structural and magnetic study of the defect perovskite LaNiO_{2.5} from high-resolution neutron diffraction data, Journal of Physics-Condensed Matter 9, 6417 (1997).
- [38] J. A. J. A. Alonso, M. J. Martinez-lope, and M. J. Martínez-Lope, Preparation and crystal structure of the deficient perovskite LaNiO_{2.5}, solved from neutron powder diffraction data, Journal of the Chemical Society, Dalton Transactions, 2819 (1995).
- [39] T. Moriga, O. Usaka, T. Imamura, I. Nakabayashi, I. Mat-

- subara, T. Kinouchi, S. Kikkawa, and F. Kanamaru, Synthesis, Crystal Structure, and Properties of Oxygen-Deficient Lanthanum Nickelate LaNiO_{3-x} ($0 \le x \le 0.5$), Bulletin of the Chemical Society of Japan **67**, 687 (1994).
- [40] A. Malashevich and S. Ismail-Beigi, First-principles study of oxygen-deficient LaNiO₃ structures, Physical Review B
 Condensed Matter and Materials Physics 92, 1 (2015).
- [41] A. M. Glazer, The classification of tilted octahedra in perovskites, Acta Crystallographica Section B 28, 3384 (1972).
- [42] Y. Matsumoto, T. Yamamoto, K. Nakano, H. Takatsu, T. Murakami, K. Hongo, R. Maezono, H. Ogino, D. Song, C. M. Brown, C. Tassel, and H. Kageyama, High-pressure synthesis of A₂NiO₂Ag₂Se₂ (A=Sr, Ba) with a high-spin Ni²⁺ in square-planar coordination, Angewandte Chemie International Edition 58, 756 (2019).
- [43] J. Goodenough, In magnetism and the chemical bond;

- cotton, fa; olah, ga; prigogine, i., eds.; interscience monographs chemistry (1963).
- [44] J. Kanamori, Superexchange interaction and symmetry properties of electron orbitals, Journal of Physics and Chemistry of Solids 10, 87 (1959).
- [45] I. I. Mazin, D. I. Khomskii, R. Lengsdorf, J. A. Alonso, W. G. Marshall, R. M. Ibberson, A. Podlesnyak, M. J. Martínez-Lope, and M. M. Abd-Elmeguid, Charge ordering as alternative to Jahn-Teller distortion, Phys. Rev. Lett. 98, 176406 (2007).
- [46] G. Giovannetti, S. Kumar, D. Khomskii, S. Picozzi, J. V. D. Brink, and J. van den Brink, Multiferroicity in rare-earth nickelates RNiO₃, Phys. Rev. Lett. 103, 156401 (2009).
- [47] B. Li, D. Louca, S. Yano, L. G. Marshall, J. Zhou, and J. B. Goodenough, Insulating pockets in metallic LaNiO₃, Advanced Electronic Materials 2, 1500261 (2016).